Geophysical Research Letters

RESEARCH LETTER
10.1029/2019GL082043

Climatic Controls on Landscape Dissection and Network Structure in the Absence of Vegetation

Milad Hooshyar[1], Arvind Singh[2], Dingbao Wang[2], and Efi Foufoula-Georgiou[3]

[1]Princeton Environmental Institute and Princeton Institute for International and Regional Studies, Princeton University, Princeton, NJ, USA, [2]Department of Civil, Environmental, and Construction Engineering, University of Central Florida, Orlando, FL, USA, [3]Department of Civil and Environmental Engineering and Department of Earth System Science, University of California, Irvine, CA, USA

Abstract Drainage networks emerge due to the movement of sediment driven by climatic and tectonic forcings. Previous observations revealed the dependence of drainage density (D_d) on climatic factors such as mean annual precipitation (MAP). Specifically, it has been observed in intermediate climate (~175 mm < MAP < 700 mm) that D_d decreases with increasing MAP. This declining trend has been argued to be attributed to biotic activity, that is, the dominance of vegetation growth over runoff erosive force. Using high-resolution topographic data from a physical experiment, we show that increasing rainfall may result in decreasing D_d even in the absence of biotic activity. Increasing rainfall rate results in narrower and less variable bifurcation angle and relatively longer links. The response of the evolving network in terms of bifurcation angle continues beyond the time when D_d has reached a new stable value, indicating that the network's topological response is relatively slower than the geomorphic response.

Key Points:
- Drainage density decreases with increasing rainfall rate in a physical experiment without vegetation
- Convergent and divergent features show distinct responses to the change in rainfall
- Higher rainfall rate results in narrower and less variable bifurcating angles and longer links

Supporting Information:
- Supporting Information S1

Correspondence to:
A. Singh,
arvind.singh@ucf.edu

Citation:
Hooshyar, M., Singh, A., Wang, D., & Foufoula-Georgiou, E. (2019). Climatic controls on landscape dissection and network structure in the absence of vegetation. *Geophysical Research Letters*, *46*. https://doi.org/10.1029/2019GL082043

Received 15 JAN 2019
Accepted 11 MAR 2019
Accepted article online 18 MAR 2019

1. Introduction

Climate and tectonic uplift shape the Earth's landscapes and the channel networks draining them (Godard et al., 2013; Singh et al., 2015; Tucker & Slingerland, 1997; Willgoose, 1994a). Understanding the response of landscapes to climatic variations is essential for predicting the climate-induced changes to Earth's surface and identifying the imprinted signatures of past climatic fluctuations (Brakenridge, 1980; Foreman et al., 2012; Jerolmack & Paola, 2010; Meyer et al., 1992; Smith et al., 2013).

Landscapes evolve through the competition between diffusive and advective sediment transport. Hillslopes form via a diffusive process often described as the mass movement of sediment driven by soil creep, discontinuous runoff, or local disturbances caused by rain splash or biotic activities (Dunne et al., 2010; Fernandes & Dietrich, 1997; Perron et al., 2008; Selby, 1982). Valleys and channels form via an advective process described as the transport of concentrated flow of water (Dietrich et al., 1993; Horton, 1945; Howard, 1994; Howard & Kerby, 1983; Smith & Bretherton, 1972; Willgoose, 1994b). The transition from diffusion-dominated hillslopes to advection-dominated channels defines the spatial extent of the drainage network which is often quantitatively described by the drainage density $D_d = \frac{L}{A}$, where L denotes the total channel length and A is the drainage area (Horton, 1932, 1945).

Observations of natural basins have shown that higher mean annual precipitation (MAP) may increase or decrease D_d depending on the overall climatic conditions, that is, in extremely arid climates with sparse vegetation, higher MAP tends to increase D_d; in intermediate climates (175 mm < MAP < 700 mm according to Melton, 1957) D_d decreases with MAP, and in humid climates, increasing MAP results in higher D_d (Abrahams, 1972; Abrahams & Ponczynski, 1984; Bandara, 1974; Daniel, 1981; Melton, 1957; Sangireddy et al., 2016). Considering the dependence of both vegetation and stream power on MAP in a numerical landscape evolution model, Collins and Bras (2010) have argued that the U-shaped trend of D_d versus MAP in intermediate and humid climates represents the transition from "vegetation-dominated" (corresponding to the decreasing trend of D_d vs. MAP across intermediate climates) to "runoff-dominated" (corresponding to the increasing trend of D_d vs. MAP across humid climates) sediment flux.

In this paper, we analyze several experimental landscapes to quantify the effects of changing rainfall intensity on the characteristics of emergent drainage networks. Using terrains obtained from the eXperimental Landscape Evolution facility at the St. Anthony Falls Laboratory at the University of Minnesota, we

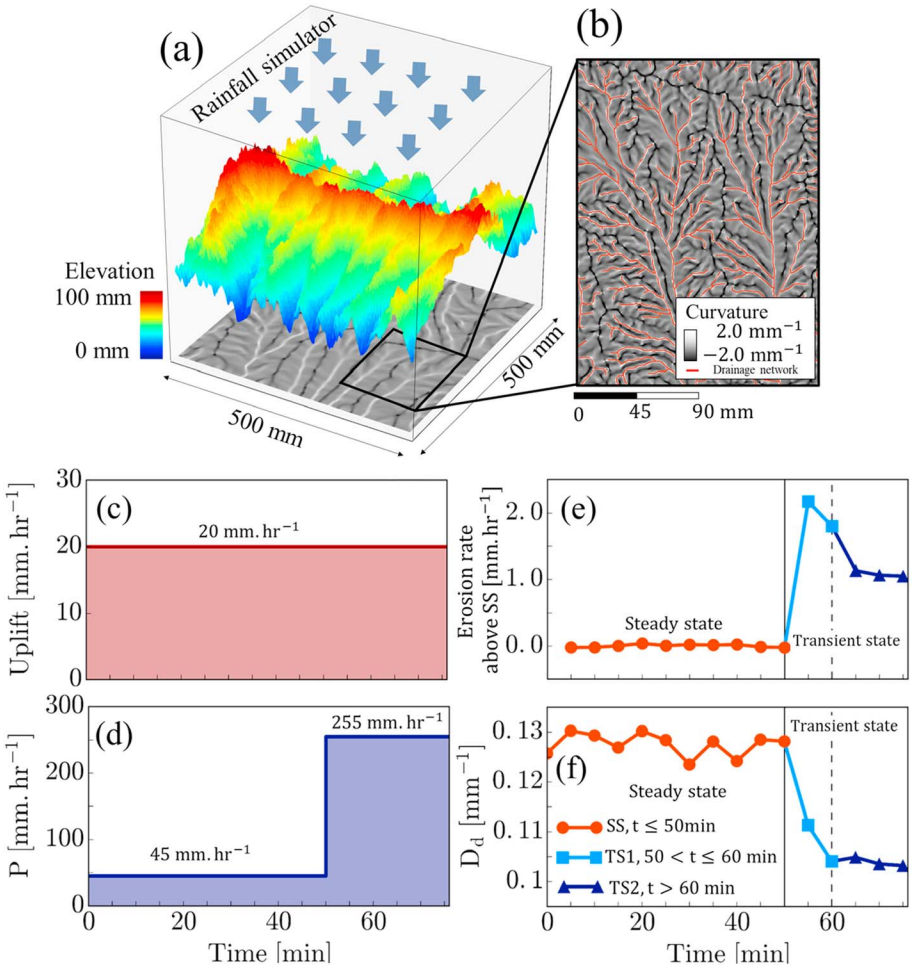

Figure 1. Experimental setup and the response to increasing rainfall. (a) The schematic view of the experimental domain and the rainfall simulator at the top. The emerged terrain at $t = 25$ min is also shown, where the colors represent elevation relative to the lowest point on the terrain. The corresponding curvature grid is projected in the horizontal plane. (b) The curvature grid and drainage network of a zoomed-in area for the terrain at $t = 25$ min. The network was extracted from 0.5 mm by 0.5 mm digital elevation model using the procedure explained in the supporting information. (c, d) The steady state (SS) landscapes emerged under a constant uplift ($U = 20$ mm/hr) and rainfall rate ($P = 45$ mm/hr). Rainfall rate was abruptly increased to 225 mm/hr at $t = 50$ min, while keeping uplift constant resulting in transient state (TS) landscapes. (e) The average erosion rate above the erosion rate of the SS landscape at $t = 50$ min. The erosion rates were computed as the averaged (over the spatial domain) elevation differences between DEMs at time t and $t = 50$ min. (f) The drainage density (D_d) decreases in response to the increase in rainfall intensity. D_d is computed as the total drainage length divided by the domain area. For further analysis, the data are grouped as SS ($t \leq 50$ min), TS1 ($50 < t \leq 60$ min), and TS2 ($t > 60$ min).

investigate the impact of precipitation on D_d and explain how the observed pattern is related to the response of the landscape in terms of convergent and divergent geomorphic features characterized by the curvature distribution. Our analysis indicates that decreasing D_d with increasing rainfall, which is observed in natural basins with intermediate climate, can still occur without vegetation. We also show how the geomorphic changes manifest in the topology and geometry of the emergent networks by studying their branching characteristics such as junction angle and link length.

2. Physical Experiments on Landscape Evolution

The experimental landscapes were obtained using the eXperimental Landscape Evolution facility at the St. Anthony Falls Laboratory at the University of Minnesota. The experimental domain was 500 mm long, 500 mm wide, and 300 mm deep (Figure 1a). The rainfall in the experiment was simulated using 20 ultrafine

misting nozzles which generated rain with droplet size <10 μm. The droplet size in this experiment was relatively small and in the form of mist, lacking sufficient energy to mobilize sediment through the splash process (Sweeney et al., 2015), giving us the confidence to assume that creep is the dominant mechanism for diffusive transport in the hillslope. The erodible material was a homogeneous mixture of fine silica (density ~ 2.65 g/cm^3) with a grain size distribution of $D_{25} = 10$ μm, $D_{50} = 25$ μm, and $D_{75} = 45$ μm, mixed with 35% water by volume in a cement mixer (refer to Singh et al., 2015, for more details). The domain was subjected to spatially uniform and temporally constant rainfall intensity ($P = 45$ mm/hr) and uplift rate ($U = 20$ mm/hr) until it reached a steady state (SS) in which the mean erosion rate was in balance with the uplift rate (Hack, 1960; Niemann & Hasbargen, 2005; Singh et al., 2015). Then, keeping uplift rate constant, the rainfall intensity was increased to 225 mm/hr (~5P), thereby shifting the landscape to a transient state (TS). High-resolution (0.5 mm by 0.5 mm) digital elevation models of the emerged terrains were acquired every 5 min using a laser scanner. Figure 1 illustrates the experimental setup.

3. Results

We analyzed 16 snapshots (landscapes) from the physical experiment at 5-min intervals spanning 75 min of simulation. For simplicity, we set $t = 0$ as the time corresponding to the first analyzed terrain which was achieved almost 8 hr after the experiment's initiation. The first 11 landscapes ($0 \le t \le 50$ min) are SS terrains which emerged under the constant rainfall (45 mm/hr) and uplift (20 mm/hr; Figure 1c) rates. The last five landscapes ($55 \le t \le 75$ min) emerged from abruptly increasing rainfall intensity to a new level of 225 mm/hr (Figure 1d) creating landscapes which are still evolving under a transient state.

We delineated drainage networks and computed D_d following the procedure explained in the supporting information (Clubb et al., 2014; Hooshyar et al., 2016; Lashermes et al., 2007; Mitasova & Hofierka, 1993; Orlandini et al., 2011; Passalacqua et al., 2010; Pelletier, 2013). Figure 1b shows the curvature grid and extracted network of a zoomed-in area in the emerged terrain at $t = 25$ min. Figure 1e shows that the SS landscape of constant erosion rate transitioned to a TS of abruptly increased erosion which subsequently decreased and approximately reached a new stable value. As shown in Figure 1f, D_d dropped significantly in response to increasing rainfall rate and reached a relatively constant value at $t = 60$ min.

We studied the probability density function (PDF) of the pixelized curvature (κ), calculated from equation S1 in the supporting information, to understand the rainfall impacts on the convergent and divergent geomorphic features (Figure 2a). The right tail of the curvature PDF in Figure 2a represents the channelized surfaces, and the left tail corresponds to the hillslopes located in upland regions. The middle part around the average (≈ 0 mm^{-1}) mostly contains the features located at the transition from hillslopes to channels.

Both tails of the curvature PDF shift downward in response to the increase in rainfall, indicating that landscapes become smoother. Higher rainfall enhances hillslope erosion and deposition in channels, reducing the proportion of pixels with high positive (channels) and negative (hillslopes) curvature in SS landscapes and increasing those with smaller curvature, leading to a narrower PDF (see Figure 2a). The smoothing effect of increasing rainfall rate also manifests in reducing the standard deviation of the curvature σ_κ. Using $|\kappa| = 0.5$ mm^{-1} as the threshold in differentiating convergent ($\kappa \ge 0.5$ mm^{-1}) and divergent ($\kappa \le -0.5$ mm^{-1}) surfaces, σ_κ decreases in response to the higher rainfall rate as demonstrated in Figure 2b. Despite this analogous behavior, the response (rate of decrease) of the convergent surfaces in terms of σ_κ is relatively large in magnitude which is also reflected in the evolution of the curvature PDF at the tails as highlighted by the downward arrows in Figure 2a. From the curvature grid of the same zoomed-in area at $t = 25$ min and $t = 75$ min shown in Figures 2c and 2d, it is evident that increasing rainfall flattens both channels and ridges, that is, reduces the absolute value of curvature. Similarly, the hillshade images in Figures 2e and 2f show how the terrain becomes smoother.

In addition, Figure 2a shows different behavior in the adjustment of the convergent and divergent surfaces to increasing rainfall, that is, the curvature in divergent surfaces adjusts fast and reaches to a new stable distribution, while in convergent surfaces it evolves gradually as shown by the downward arrows.

We studied the structure and geometry of the junctions to reveal how climate-induced geomorphic changes manifest in the topology of the emerged networks. As schematically illustrated in Figure 3a (inset), a junction can be described by its angle (α) and the length of the intersecting links (l).

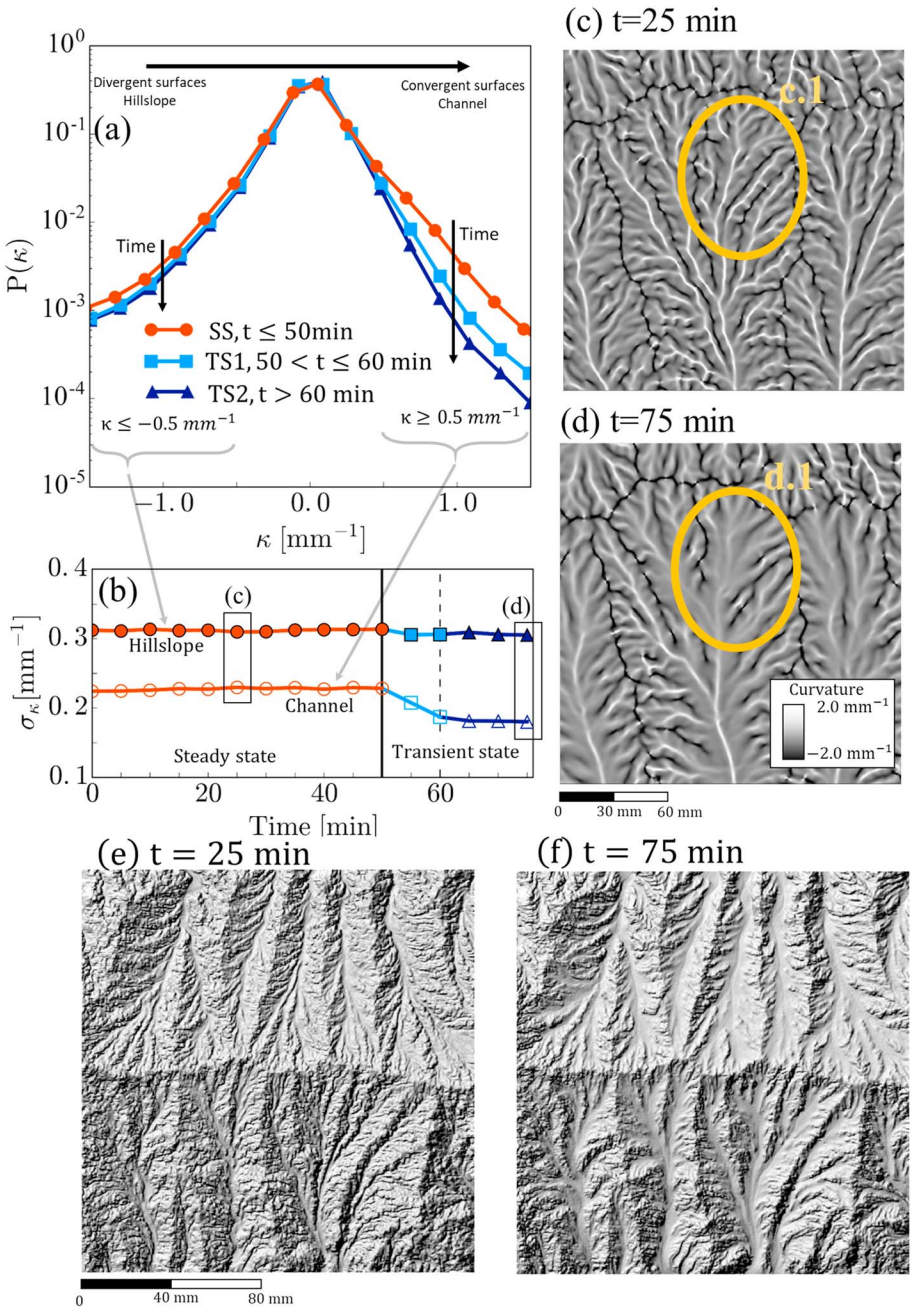

Figure 2. Effects of increasing rainfall intensity on surface curvature. (a) The probability distribution of curvature κ with bin size 0.2 mm^{-1}. The data are grouped as SS ($t \leq 50$ min), TS1 ($50 < t \leq 60$ min), and TS2 ($t > 60$ min). Higher rainfall intensity smooths the terrain and moves pixels from both tails of the probability density function toward zero curvature. (b) The standard deviation of curvature (σ_κ) for pixels with $\kappa \geq 0.5$ mm^{-1} (convergent surface) and $\kappa \leq -0.5$ mm^{-1} (divergent surface). σ_κ decreases as the landscape is forced into TS by increasing rainfall for both divergent and convergent surfaces; however, σ_κ changes with a higher rate in convergent topography. The curvature of the same zoomed-in area at $t = 25$ min (c) and $t = 75$ min (d), respectively. It is visually evident that increasing rainfall reduces the absolute curvature ($|\kappa|$) in channels (light color) and ridges (dark color) as highlighted in c.1 and d.1. The smoothing effect of the increased rainfall is visually evident in (e) and (f) which show the hillshade image generated from the gridded elevation surface at SS ($t = 25$ min) and TS ($t = 75$ min), respectively. SS = steady state; TS = transient state.

Increasing rainfall results in relatively longer links as demonstrated in the PDF of the links' length (Figure 3a) and the evolution of the average length through time (Figure 3b). On the other hand, the link density (L_d), defined as $^{N_L}/_{A}$ where N_L denotes the total number of links and A is the total area, decreases

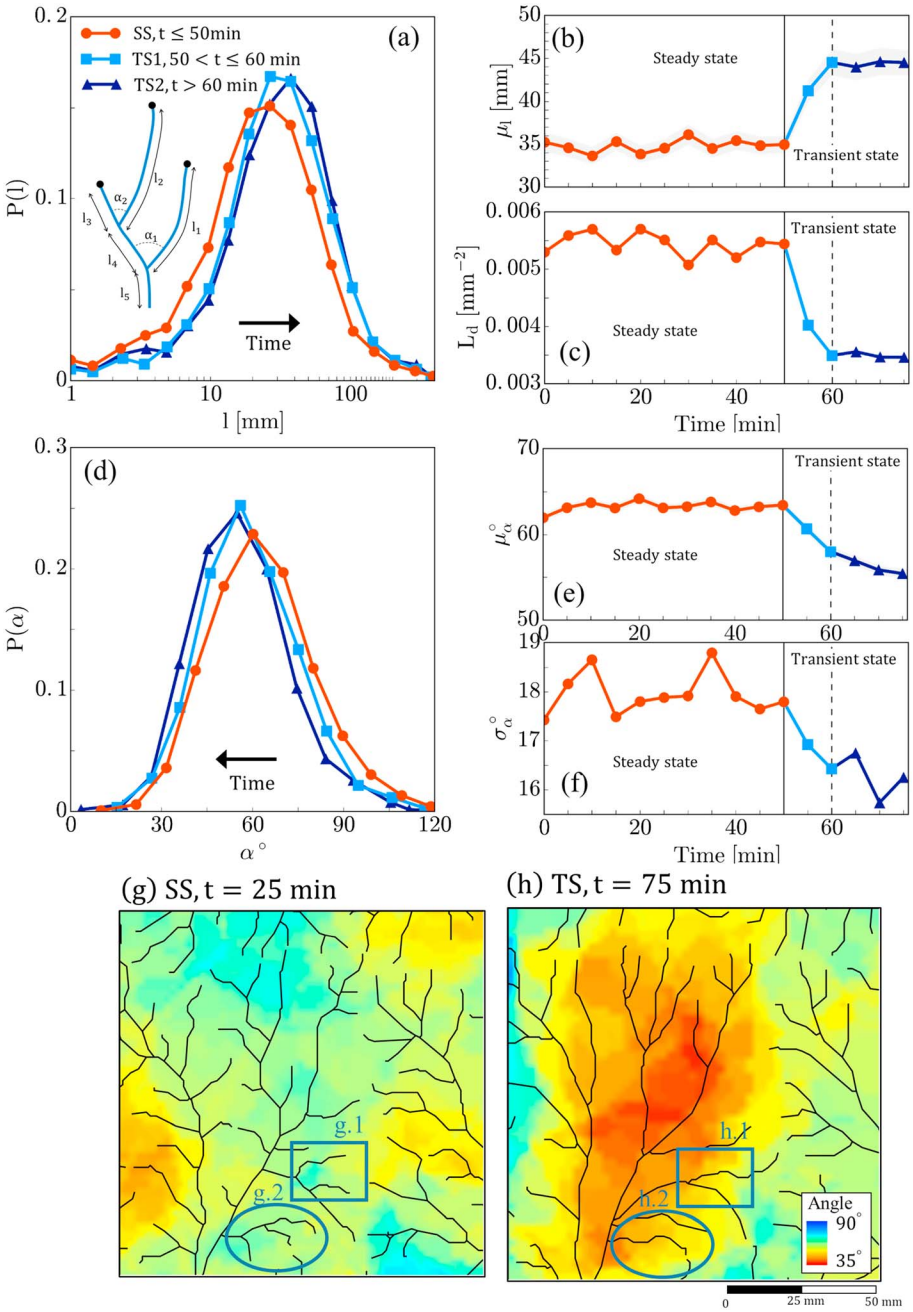

Figure 3. The effect of increasing rainfall intensity on network topology in terms of link length (l) and branching angle (α). Links and branching angles are shown schematically in the inset of panel (a) where the black dots show the channel initiation points (i.e., channel heads). The data are grouped as SS ($t \leq 50$ min), TS1 ($50 < t \leq 60$ min), and TS2 ($t > 60$ min). (a) The probability density functions (PDFs) of the link length. The general shift to the right of the PDFs implies the links' elongation in response to increasing rainfall. This is also evident in (b), which shows the evolution of the average link length (μ_l). μ_l increases by ~28% in response to the increase in rainfall. (c) The link density (L_d), defined as N_L/A, where N_L is the total number of links and A is the total drainage area, decreases in response to increasing rainfall. (d) The PDF of the junction angles, which shifts to the left and becomes narrower as rainfall increases, implies that the junctions narrow and exhibit less variation in their angles when the landscape is exposed to higher rainfall intensity. (e, f) The evolution of the average angle (μ_α) and the standard deviation of angles (σ_α), respectively. On average, the junction angles decrease by 8% in response to higher rainfall. The shaded area in (b) and (e) corresponds to the average ± standard error. (g, h) A portion of the drainage network at $t = 25$ min and $t = 75$ min, respectively. We extracted the angles for each junction to form a set of scattered points and then used kriging (Kitanidis, 1997) to generate the angle grid shown in the background for demonstration purposes. Panels (g) and (h) also highlight two cases where some links disappear in response to increasing rainfall intensity (see circles and squares). SS = steady state; TS = transient state.

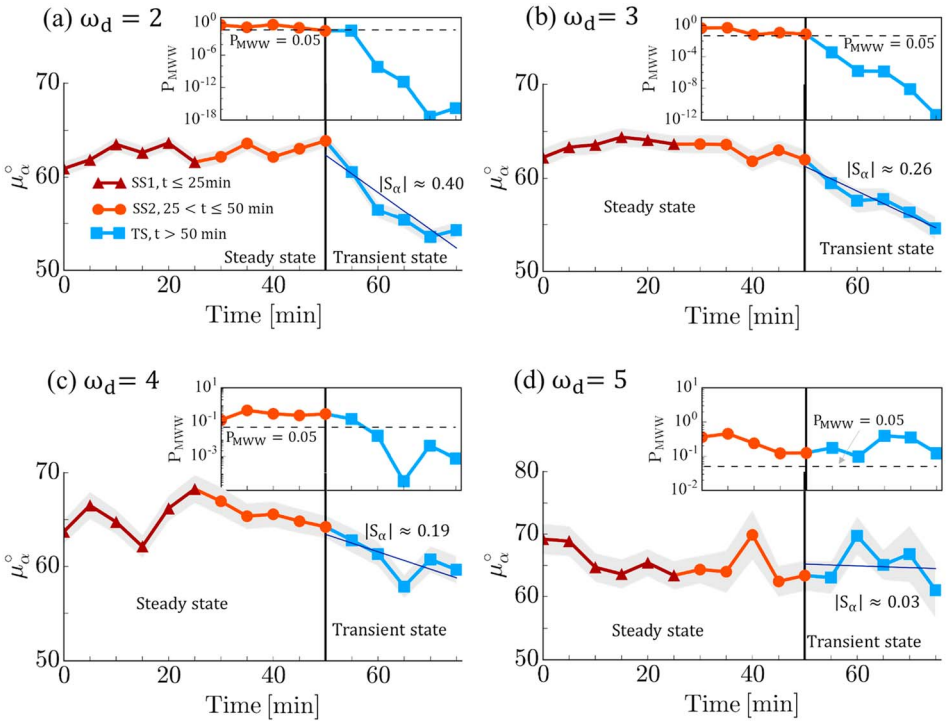

Figure 4. Evolution of junction angle across scales. (a–d) The average junction angle (μ_α) over time for $\omega_d = 2$, 3, 4, and 5, respectively, where ω_d is the Strahler (1953) order of the downstream link at each junction. On the top, the P value of the Mann-Whitney-Wilcoxon test (P_{MWW}) is shown. $P_{\mathrm{MWW}} = 0.05$ (0.05 confidence level) is marked by the dashed lines. The MWW test examines whether the angle distribution at each time deviates statistically from the reference distribution, defined as the distribution of all angles from terrains at $t \leq 25$ min (denoted by SS1). Panels (a–d) also show the slopes of the linear fits to μ_α versus time curves for $t > 50$. The decline rate of the average angle, i.e., $|S_\alpha|$, decreases with increasing basin order. The shaded area corresponds to the average angle ± standard error. The average number of junctions (averaged over 16 landscapes) were 531, 264, 136, and 39 for $\omega_d = 2$, 3, 4, and 5; respectively. MWW = Mann-Whitney-Wilcoxon.

substantially (Figure 3c). In general, higher rainfall rate results in longer but fewer links which is consistent with the decrease in D_d shown in Figure 1f.

We computed the junction angles of the extracted networks following the procedure described in the supporting information (Hooshyar et al., 2017; Ranjbar et al., 2018). As depicted in Figure 3d, the PDF of the junction angles shifts toward the left as rainfall increases. Figures 3e and 3f, which show the evolution of the average (μ_α) and standard deviation (σ_α) of angles through time, demonstrate that the channels in TS landscapes, emerging under more intense rainfall, exhibit smaller angles with less variation compared to those in SS.

The average junction angle declines gradually as rainfall increases and evolution continues for $t \geq 60$ min (Figure 3e). In contrast, D_d decreases abruptly and reaches a new stable value at $t = 60$ min (Figure 1f). This indicates that the network's topologic response to the climatic alteration is relatively slower than the geomorphic response and that it continues beyond the time when geomorphic features such as D_d reaches SS.

Figures 3g and 3h show the drainage network and junction angle for two zoomed-in areas at $t = 25$ min and $t = 75$ min, respectively. These two examples clearly demonstrate how the junction angles narrow and the links disappear in response to increasing rainfall.

Junctions are formed when two upstream links merge to a single downstream link. Here, we categorized junctions based on the Strahler (1953) order of the downstream link, denoted by ω_d. For example, the junction marked by α_2 in the inset of Figure 3a has $\omega_d = 2$ since its downstream link, marked by l_4, is a second-order channel. Figure 4 shows the evolution of the average angle through time for $\omega_d = 2$, 3, 4, and 5. Selecting terrains at $t \leq 25$ min (first six snapshots at SS, denoted by SS1) as the reference, we performed a

Mann-Whitney-Wilcoxon (Mann & Whitney, 1947; Wilcoxon, 1945) test to check whether the angle distribution at each snapshot at $t > 25$ min differs statistically from the reference distribution of the angles. In Figure 4, the P value of the Mann-Whitney-Wilcoxon test, denoted by P_{MWW}, clearly shows that the angles at SS do not differ statistically from the reference angles across scale (i.e., for different ω_d). However, for $\omega_d = 2$ and 3 at $t \geq 55$ min and for $\omega_d = 4$ at $t \geq 60$ min , the angle distribution deviates significantly from the reference distribution at the 0.05 confidence level. The P_{MWW} curve shows an insignificant difference for higher scale $\omega_d = 5$, suggesting that the effect of changing precipitation is mainly confined to smaller-order channels as opposed to larger ones. Finally, the absolute slope of linear fits to μ_α versus time curves for $t > 50$ min , that is, after increasing rainfall rate, denoted by $|S_\alpha|$, indicates that the declining rate of average angle decreases with scale. In other words, the perturbations induced by increasing rainfall propagate through the network from smaller to higher orders in terms of junction angles.

4. Discussion and Conclusions

The drainage density in natural basins with intermediate climate (175 mm < MAP < 700 mm according to Melton, 1957) shows a strongly declining trend with MAP (Sangireddy et al., 2016), or precipitation effectiveness index (Melton, 1957), defined as 10 multiplied by the annual summation of ratios between monthly average precipitation and evaporation (Thornthwaite, 1931). Scaling analysis indicates that the physical experiment at SS with $P \approx 45$ mm/hr corresponds roughly to MAP ≈ 250 mm/year, which is within the range for the intermediate climate (see supporting information for more details; Perron et al., 2008; Perron et al., 2009; Shelef & Hilley, 2014; Singh et al., 2015; Sweeney et al., 2015; Tarboton, 1997; Willgoose et al., 1991).

The decreasing trend of D_d with MAP (or precipitation effectiveness index) in natural basins has been explained considering the competition between rainfall erosive and vegetation resistive forces. Some studies suggested that as the rainfall increases the vegetation gets denser which further stabilizes the land surface and provides more resistance to erosion. This upsurge in soil resistance suppresses the escalation in erosive force of rainfall leading to lower D_d (Abrahams, 1984; Collins & Bras, 2010; Istanbulluoglu & Bras, 2005). Although a similar declining trend in D_d with respect to MAP was observed in the experiment, the physical processes are different because the experiment lacked vegetation cover. It was observed that higher rainfall causes more erosion on the hillslopes. The eroded material is transported downslope because of the runoff resulting in transport-limited (in particular, sediment-flux dependent; Whipple & Tucker, 2002) conditions in the channels (see Singh et al., 2015; Tejedor et al., 2017). The erosion from hillslopes and deposition in channels smooth the landscape as the ridges erode and the channels become shallower. Some ridges and channels disappear altogether, leading to decreased D_d. These processes were also evident in the curvature distribution as it narrows (smaller σ_κ) in response to greater amounts of rainfall.

The curvature in divergent surfaces approaches a new stable distribution relatively fast while in convergent surfaces; the evolution continues for a relatively longer time. Divergent hilltops are formed by diffusive transport, which is controlled by the local properties of the surface (curvature), whereas the formation of channels depends on both the local (slope) and nonlocal characteristics of the surface (discharge and deposition of eroded material from upstream). The nonlocal controls on channel formation may contribute to the longer response time of the convergent surfaces.

Our analysis further reveals the climatic controls on the network structure. Specifically, increased rainfall rate results in a network with smaller junction angles and relatively longer and fewer links. Observation from natural drainage networks has shown that the channels in humid climates tend to branch at higher angles due to the dominance of groundwater seepage in the formation and growth of channels (Seybold et al., 2017). However, the sediment transport in our experiment is driven solely based on surface runoff with no groundwater seepage.

The decrease in the number of links is partially due to the filling (and thus removal) of channels through the deposition of eroded sediment from hillslopes under increasing rainfall intensity. The network's response with respect to junction angle is evident up to a scale $\omega_d = 4$, where ω_d is the Strahler (1953) order of the downstream link at each junction. At a lower scale (smaller ω_d), the junction angles exhibit a relative steep decay compared to higher orders. This implies a scale control on the rate of change in junction angles in response to increased precipitation.

The $\frac{D_r}{D_{50}}$ ratio (D_r is the rain droplet size, and D_{50} describes erodible material particle size) in our experiment was <0.4, which may be smaller than that of natural basins (assuming rain droplet size of 1.0 mm). The erodible material also differs from the natural soil in terms of particle heterogeneity and chemical properties, which may affect the erodibility. Our main criterion for selecting the grain size was to make sure we obtain a well-defined channel network in such a small experiment basin by testing several alternatives.

The rainfall in the experiment was uniform in space and time; however, climatic forcing naturally consists of spatially nonuniform events with variable duration and magnitude. The material was saturated before and throughout the experiment with no vegetation cover; therefore, our experiment lacked hydrologic processes such as infiltration, groundwater seepage, and evaporation. In addition, several small-scale characteristics of the experiment such as surface tension effects and laminar flow at streams may not be directly extendable to natural basins.

The experimental landscapes contained both fluvial and colluvial regimes similar to those observed in natural basins (see, e.g., Figure S1 in supporting information for the landscape at $t = 20$ min). However, the concavity indices (0.1 and 0.3 for colluvial and fluvial regimes in Figure S1) were slightly smaller than those observed in natural basins, suggesting that the experiment was more representative of relatively steep channels fed by surface runoff than fairly flat perennial streams.

Acknowledgments
M. H. acknowledges the support from the University of Central Florida (through the P3 postdoctoral program), the National Center for Earth-Surface Dynamics (through NCED2 (NSF EAR-1246761) Synthesis postdoctoral fellowship), and the University of Central Florida Stokes Advanced Research Computing Center for providing computational resources. The authors thank the Editor M. Bayani Cardenas, Wolfgang Schwanghart, and two anonymous reviewers for their constructive comments and suggestions that have helped substantially in improving our presentation and refining our interpretations. The DEMs for the emerged surfaces can be found at https://www.hydroshare.org/resource/a40b43d8734947d3a9871434c173230c.

References

Abrahams, A. (1972). Drainage densities and sediment yields in eastern Australia. *Geographical Research*, *10*(1), 19–41.
Abrahams, A. (1984). Channel networks: A geomorphological perspective. *Water Resources Research*, *20*(2), 161–188. https://doi.org/10.1029/WR020i002p00161
Abrahams, A., & Ponczynski, J. (1984). Drainage density in relation to precipitation intensity in the USA. *Journal of Hydrology*, *75*(1–4), 383–388. https://doi.org/10.1016/0022-1694(84)90061-1
Bandara, M. (1974). Drainage density and effective precipitation. *Journal of Hydrology*, *21*(2), 187–190. https://doi.org/10.1016/0022-1694(74)90036-5
Brakenridge, R. (1980). Widespread episodes of stream erosion during the Holocene and their climatic cause. *Nature*, *283*(5748), 655–656. https://doi.org/10.1038/283655a0
Clubb, F. J., Mudd, S. M., Milodowski, D. T., Hurst, M. D., & Slater, L. J. (2014). Objective extraction of channel heads from high-resolution topographic data. *Water Resources Research*, *50*, 4283–4304. https://doi.org/10.1002/2013WR015167
Collins, D., & Bras, R. (2010). Climatic and ecological controls of equilibrium drainage density, relief, and channel concavity in dry lands. *Water Resources Research*, *46*, W04508. https://doi.org/10.1029/2009WR008615
Daniel, J. (1981). Drainage density as an index of climatic geomorphology. *Journal of Hydrology*, *50*, 147–154. https://doi.org/10.1016/0022-1694(81)90065-2
Dietrich, W., Wilson, C., Montgomery, D., & McKean, J. (1993). Analysis of erosion thresholds, channel networks, and landscape morphology using a digital terrain model. *Journal of Geology*, *101*(2), 259–278.
Dunne, T., Malmon, D., & Mudd, S. (2010). A rain splash transport equation assimilating field and laboratory measurements. *Journal of Geophysical Research*, *115*, F01001. https://doi.org/10.1029/2009JF001302
Fernandes, N., & Dietrich, W. (1997). Hillslope evolution by diffusive processes: The timescale for equilibrium adjustments. *Water Resources Research*, *33*(6), 1307–1318. https://doi.org/10.1029/97WR00534
Foreman, B., Heller, P., & Clementz, M. (2012). Fluvial response to abrupt global warming at the Palaeocene/Eocene boundary. *Nature*, *491*(7422), 92–95. https://doi.org/10.1038/nature11513
Godard, V., Tucker, G., Burch Fisher, G., Burbank, D., & Bookhagen, B. (2013). Frequency-dependent landscape response to climatic forcing. *Geophysical Research Letters*, *40*, 859–863. https://doi.org/10.1002/grl.50253
Hack, J. (1960). Interpretation of erosional topography in humid temperate regions. *American Journal of Science*, *258-A*, 80–97.
Hooshyar, M., Singh, A., & Wang, D. (2017). Hydrologic controls on junction angle of river networks. *Water Resources Research*, *53*, 4073–4083. https://doi.org/10.1002/2016WR020267
Hooshyar, M., Wang, D., Kim, S., Medeiros, S. C., & Hagen, S. C. (2016). Valley and channel networks extraction based on local topographic curvature and k-means clustering of contours. *Water Resources Research*, *52*, 8081–8102. https://doi.org/10.1002/2015WR018479
Horton, R. (1932). Drainage-basin characteristics. *Transactions of the American Geophysical Union*, *13*(1), 350–361. https://doi.org/10.1029/TR013i001p00350
Horton, R. (1945). Erosional development of streams and their drainage basins; hydrophysical approach to quantitative morphology. *Geological Society of America Bulletin*, *56*(3), 275–370. https://doi.org/10.1130/0016-7606(1945)56[275:EDOSAT]2.0.CO;2
Howard, A. (1994). A detachment-limited model of drainage basin evolution. *Water Resources Research*, *30*(7), 2261–2285. https://doi.org/10.1029/94WR00757
Howard, A., & Kerby, G. (1983). Channel changes in badlands. *Geological Society of America Bulletin*, *94*(6), 739–752. https://doi.org/10.1130/0016-7606(1983)94<739:CCIB>2.0.CO;2
Istanbulluoglu, E., & Bras, R. (2005). Vegetation-modulated landscape evolution: Effects of vegetation on landscape processes, drainage density, and topography. *Journal of Geophysical Research*, *110*, F02012. https://doi.org/10.1029/2004JF000249
Jerolmack, D., & Paola, C. (2010). Shredding of environmental signals by sediment transport. *Geophysical Research Letters*, *37*, L19401. https://doi.org/10.1029/2010GL044638
Kitanidis, P. (1997). *Introduction to geostatistics: Applications in hydrogeology*. Cambridge, UK: Cambridge University Press. https://doi.org/10.1017/CBO9780511626166
Lashermes, B., Foufoula-Georgiou, E., & Dietrich, W. E. (2007). Channel network extraction from high resolution topography using wavelets. *Geophysical Research Letters*, *34*, L23S04. https://doi.org/10.1029/2007GL031140

Mann, H., & Whitney, D. (1947). On a test of whether one of two random variables is stochastically larger than the other. *The Annals of Mathematical Statistics*, *18*(1), 50–60.
Melton, M. (1957). *An analysis of the relations among elements of climate, surface properties, and eomorphology*. New York: Columbia University, Department of Geology.
Meyer, G., Wells, S., Balling, R., & Jull, T. (1992). Response of alluvial systems to fire and climate change in Yellowstone National Park. *Nature*, *357*(6374), 147–150. https://doi.org/10.1038/357147a0
Mitasova, H., & Hofierka, J. (1993). Interpolation by regularized spline with tension: II. Application to terrain modeling and surface geometry analysis. *Mathematical Geology*, *25*(6), 657–669.
Niemann, J. D., & Hasbargen, L. E. (2005). A comparison of experimental and natural drainage basin morphology across a range of scales. *Journal of Geophysical Research*, *110*, F04017. https://doi.org/10.1029/2004JF000204
Orlandini, S., Tarolli, P., Moretti, G., & Dalla Fontana, G. (2011). On the prediction of channel heads in a complex alpine terrain using gridded elevation data. *Water Resources Research*, *47*, W02538. https://doi.org/10.1029/2010WR009648
Passalacqua, P., Do Trung, T., Foufoula-Georgiou, E., Sapiro, G., & Dietrich, W. E. (2010). A geometric framework for channel network extraction from lidar: Nonlinear diffusion and geodesic paths. *Journal of Geophysical Research*, *115*, F01002. https://doi.org/10.1029/2009JF001254
Pelletier, J. D. (2013). A robust, two-parameter method for the extraction of drainage networks from high-resolution digital elevation models (DEMs): Evaluation using synthetic and real-world DEMs. *Water Resources Research*, *49*, 75–89. https://doi.org/10.1029/2012WR012452
Perron, T., Dietrich, W., & Kirchner, J. (2008). Controls on the spacing of first-order valleys. *Journal of Geophysical Research*, *113*, F04016. https://doi.org/10.1029/2007JF000977
Perron, T., Kirchner, J., & Dietrich, W. (2009). Formation of evenly spaced ridges and valleys. *Nature*, *460*(7254), 502–505. https://doi.org/10.1038/nature08174
Ranjbar, S., Hooshyar, M., Singh, A., & Wang, D. (2018). Quantifying climatic controls on river network branching structure across scales. *Water Resources Research*, *54*, 7347–7360. https://doi.org/10.1029/2018WR022853
Sangireddy, H., Carothers, R., Stark, C., & Passalacqua, P. (2016). Controls of climate, topography, vegetation, and lithology on drainage density extracted from high resolution topography data. *Journal of Hydrology*, *537*, 271–282. https://doi.org/10.1016/j.jhydrol.2016.02.051
Selby, M. (1982). *Hillslope materials and processes* (2nd ed., p. 451). Oxford: Oxford University Press.
Seybold, H., Rothman, D. H., & Kirchner, J. W. (2017). Climate's watermark in the geometry of stream networks. *Geophysical Research Letters*, *44*, 2272–2280. https://doi.org/10.1002/2016GL072089
Shelef, E., & Hilley, G. E. (2014). Symmetry, randomness, and process in the structure of branched channel networks. *Geophysical Research Letters*, *41*, 3485–3493. https://doi.org/10.1002/2014GL059816
Singh, A., Reinhardt, L., & Foufoula-Georgiou, E. (2015). Landscape reorganization under changing climatic forcing: Results from an experimental landscape. *Water Resources Research*, *51*, 4320–4337. https://doi.org/10.1002/2015WR017161
Smith, T., & Bretherton, F. (1972). Stability and the conservation of mass in drainage basin evolution. *Water Resources Research*, *8*(6), 1506–1529. https://doi.org/10.1029/WR008i006p01506
Smith, V., David, C., Cardenas, B., & Yang, Z. (2013). Climate, river network, and vegetation cover relationships across a climate gradient and their potential for predicting effects of decadal-scale climate change. *Journal of Hydrology*, *488*, 101–109. https://doi.org/10.1016/j.jhydrol.2013.02.050
Strahler, A. (1953). Revisions of Horton's quantitative factors in erosional terrain. *Transactions of the American Geophysical Union*, *34*, 345.
Sweeney, K., Roering, J., & Ellis, C. (2015). Experimental evidence for hillslope control of landscape scale. *Science*, *349*(6243), 51–53. https://doi.org/10.1126/science.aab0017
Tarboton, D. (1997). A new method for the determination of flow directions and upslope areas in grid digital elevation models. *Water Resources Research*, *33*(2), 309–319. https://doi.org/10.1029/96WR03137
Tejedor, A., Singh, A., Zaliapin, I., Densmore, A., & Foufoula-Georgiou, E. (2017). Scale-dependent erosional patterns in steady-state and transient-state landscapes. *Science Advances*, *3*(9), e1701683. https://doi.org/10.1126/sciadv.1701683
Thornthwaite, W. (1931). The climates of North America: According to a new classification. *Geographical Review*, *21*, 633–655.
Tucker, G., & Slingerland, R. (1997). Drainage basin responses to climate change. *Water Resources Research*, *33*(8), 2031–2047. https://doi.org/10.1029/97WR00409
Whipple, K. X., & Tucker, G. E. (2002). Implications of sediment-flux-dependent river incision models for landscape evolution. *Journal of Geophysical Research*, *107*(B2), 2039. https://doi.org/10.1029/2000JB000044
Wilcoxon, F. (1945). Individual comparisons by ranking methods. *Biometrics Bulletin*, *1*(6), 80–83. https://doi.org/10.2307/3001968
Willgoose, G. (1994a). A statistic for testing the elevation characteristics of landscape simulation models. *Journal of Geophysical Research*, *99*(B7), 13,987–13,996. https://doi.org/10.1029/94JB00123
Willgoose, G. (1994b). A physical explanation for an observed area-slope-elevation relationship for catchments with declining relief. *Water Resources Research*, *30*(2), 151–159. https://doi.org/10.1029/93WR01810
Willgoose, G., Bras, R., & Rodriguez-Iturbe, I. (1991). Results from a new model of river basin evolution. *Earth Surface Processes and Landforms*, *16*(3), 237–254. https://doi.org/10.1002/esp.3290160305